

Determining the thermal capacitance, conductivity and the convective heat transfer coefficient of a brick wall by annually monitored temperatures and total heat fluxes

C. Luo, B. Moghtaderi*, S. Hands, A. Page

Priority Research Centre for Energy, School of Engineering, Faculty of Engineering & Built Environment, The University of Newcastle, University Drive, Callaghan, NSW 2308, Australia

ARTICLE INFO

Article history:

Received 12 July 2010

Accepted 29 September 2010

Keywords:

Thermal capacitance

Convective heat transfer coefficient

Thermal conductivity

Thermal radiation

Finite volume

Total exchange area

ABSTRACT

The finite volume scheme and complex Fourier analysis methods are proposed to determine the thermal capacitance (defined as the product of density and specific capacity) and thermal conductivity for a building construction layer using the monitored inner/outer surface temperatures and heat fluxes. The overall heat transfer coefficient for the air gap, and the convective heat transfer coefficient for air gap surfaces and room surfaces are determined by the linear relationship between the surface convective heat flux and the temperature difference. Convective heat flux is obtained by removing the thermal radiation flux from the total surface heat flux. Finally, the predicted surface heat fluxes using the calculated thermal properties and ASHRAE values were compared with the measurements.

© 2010 Elsevier B.V. All rights reserved.

1. Introduction

For any energy simulation (ES) software the basic input parameters required for a material are the thermal conductivity or heat resistance and the thermal capacitance, which is defined as the product of density and heat capacity. Measuring the thermal conductivity of a material as a walling system requires use of laboratory controlled and natural climatic conditions to create differing climates for both wall surfaces. ASTM C518-04 [1] requires steady state conditions across the test specimen allowing the thermal conductivity to be calculated by the measured steady state heat flux and surface temperatures. Compared to the original guarded hot box method ASTM C1363-05 [2] which determines the steady heat flux by the heat input from fan and coil elements, ASTM C518-04 directly measures the steady state heat flux by a heat flux transducer. Steady state conditions across the tested walling system can only be established in laboratory controlled conditions through heating or cooling. However as initial conditions for the tested building walls differ from the target steady state conditions, it will take some time to establish the desired steady state conditions across the testing walls. Gustafsson [3] and Bouguerra et al. [4] measured thermal conductivity and diffusivity by correlating the

electric resistance of the transient plane source heating element with the thermal properties of the tested specimen. Although it is only necessary to record the transient temperature variation history for the transient plane source (TPS) method, it is still classified as a laboratory controlled climate as the TPS element requires heating. Ghazi et al. [5] used a heat flow meter apparatus (HFM) to measure three temperatures at lower, middle and upper heights of two specimens and determined the specific heat capacity of the specimen by comparing the thermal simulation using three different values of C_p with the measured response (the temperature at the middle of the two species). Steady state conditions across the tested specimen are required for ASTM C518-04, ASTM C1363-05 and the HFM but not for the transient plane source method.

One of the disadvantages of measuring the thermal properties under a laboratory-controlled climate is that the tested specimen would then be placed within a natural actual climate which differs from the testing conditions. Thermal properties such as and especially the thermal conductivity are dependent on climatic effects including humidity and solar radiation. Accordingly, some researchers began seeking a derivation for the thermal properties based upon in-situ measurements such as surface temperatures and heat fluxes. Carpentier et al. [6] calculated the thermal diffusivity of the soil based on the monitored temperatures at the ground surface and at a location below the surface. Further, they obtained the thermal conductivity of the soil by the relationship between the amplitudes of the surface temperature and heat

* Corresponding author. Tel.: +61 2 49854411; fax: +61 2 49216893.

E-mail address: Behdad.Moghtaderi@newcastle.edu.au (B. Moghtaderi).

Nomenclature

$a, a_1, b, b_1, c, c_1, d_1$	intermediate variable for solving thermal conductivity
A	cross section area (m^2)
C_a	thermal capacitance ($J/m^3 K$)
C_{Ti}	complex Fourier expansion amplitude for temperature (K)
C_p	specific heat at constant pressure ($J/kg K$)
C_{Qi}	complex Fourier expansion amplitude for heat flux (W/m^2)
h	heat transfer coefficient ($W/m^2 K$)
H	complex number
j	complex imaginary unit
k	thermal conductivity ($W/m K$)
L_t	thickness of the construction material layer (m)
P	period (s)
psd	power spectral density
\dot{q}''	surface heat flux (W/m^2)
Q	complex Fourier expansion amplitude for surface heat flux (W/m^2)
R	thermal resistance ($m^2 K/W$)
S	total exchange area (m^2)
t	time (s, min or h)
T	temperature (K or $^{\circ}C$) or complex Fourier expansion amplitude
U	overall heat transfer coefficient ($W/m^2 K$)
x	spatial coordinate (m)
X_i	Fourier expansion coefficient
Y_i	Fourier expansion coefficient
ε	thermal radiation emissivity (-)
σ	Stefan-Boltzmann constant ($W/m^2 K^4$)
ϕ	any temporal-varying variable
ω	angular frequency ($1/s$)
Δt	time step (s, min or h)
Δx	spatial step (m)

Subscripts

conv	convective
e	external surface
G	ground
i	inner surface, or surface index
j	surface index
N	north
ra	room air
$s0$	left wall surface (or outer surface)
$s1$	right wall surface (or inner surface)
t	total
w	wall

flux. Peng and Wu [7] introduced three methods to evaluate the total thermal resistance of a building wall based on the internal and external average air temperatures, internal and external surface average temperatures, inner surface average heat flux and average solar radiant illumination. Cucumo et al. [8] evaluated the wall conductance in terms of the internal wall surface heat flux and the internal and external surface temperatures using the finite difference calculation code. They calculated the inner wall surface heat flux under different equivalent wall thermal conductivities and equivalent thermal capacities using the internal and external surface temperatures as inputs, compared their predictions with measurements and selected the equivalent wall thermal conductivity and equivalent thermal capacity based on the best match between the predictions and measurements.

Emmel et al. [9], Hagishima and Tanimoto [10], Jayamaha et al. [11], Liu and Harris [12], Shao et al. [13] measured the convective heat transfer coefficient (CHTC) of the outer building wall surface under different environmental conditions. The CHTC on the outside wall surface depends on the building geometry, wind speed and wind direction. The CHTC of the inner wall surface does not directly depend on the weather conditions, but on the air movement induced by the internal temperature distribution, which could source from forced air circulation using an electric fan, construction wall infiltration or ventilation. Irving et al. [14] and Delaforce et al. [15] obtained the CHTC through the correlation between the surface heat flux and the temperature difference between the wall surface and the indoor air temperature (in the boundary layer of wall surface) measured by the Meyer ladder.

This study is not aimed at improving the measuring techniques as mentioned above, but focused on calculating the thermal capacitance, thermal conductivity and convective heat transfer coefficients during monitoring of the thermal performance of buildings. Accordingly, the thermal properties (thermal capacitance and thermal conductivity) for homogeneous building materials are determined by in-situ (not laboratory-controlled conditions) measurements using the finite volume and complex Fourier analysis methods for the wall construction. The CHTC is obtained by linear fitting for building wall surfaces surround and air gaps. The effect of the thermal radiation on the CHTC for the indoor wall surfaces is also investigated and the predicted room air temperatures using the fitted thermal properties and the ASHRAE table values will be compared with the measurements.

2. Instrumentation of modules

The experimental data was obtained from fully instrumented $6 m \times 6 m$ test modules located on the University of Newcastle campus which were constructed to measure and compare the thermal performance of various walling systems under natural conditions. The instrumentation recorded the external weather conditions; wind speed and direction, air temperature, relative humidity and, the incident solar radiation on each wall (vertical-plane) and the horizontal plane. For each module, temperature and heat flux profiles through the walls, slab and ceiling were recorded in conjunction with the internal air temperature and relative humidity. Approximately 105 data channels were scanned and logged every 10 min for each of the modules all year round. The data was recorded using Datataker DT600 data loggers with three 30 channel expansion modules located in each building. All temperatures were measured using Type T thermocouples. Thermocouple inputs were maintained at a uniform temperature through the use of a thick wall aluminium isothermal box to minimise cold junction compensation errors and temperature gradients across the loggers. The temperature recording system (thermocouple wire characteristics, cold junction compensation, etc.) was cross-referenced using a Prema Precision Thermometer and the corresponding temperature offsets were compensated for during the logging process.

Heat fluxes through the module surfaces were measured with $100 mm \times 100 mm$ thermopile sensors with typical sensitivities in the order of $25 \mu V/W/m^2$. The heat flux sensors were placed on the wall in such a manner that the masonry unit/mortar ratio recorded was representative of the entire masonry wall. An attempt was made to match the absorbance and emissivity of the heat flux sensors to that of the masonry units by painting the exterior sensors a similar colour and finish to that of the bricks. The interior sensors were painted white, to match the walls, whilst the sensors located in the cavities were painted black to allow radiative heat transfer. Fig. 1 shows the typical sensor layout for the brick veneer wall.

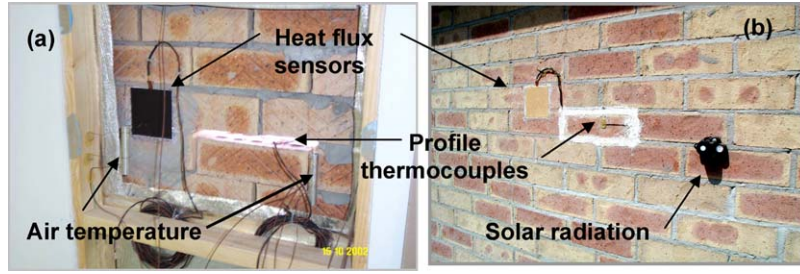


Fig. 1. Wall sensors used in the brick veneer wall, (a) internal and (b) external.

3. Mathematical expressions

3.1. Calculating thermal capacitance and thermal conductivity by the finite volume method

For any construction material layer, the heat flux and temperature at both layer surfaces can be correlated by the following two equations as illustrated by Luo et al. [16]:

$$\frac{1}{162k} L_t^2 \rho C_p \left[\left(57T_e + 24T_i - \frac{9L_t}{k} q_e'' + \frac{6L_t}{k} q_i'' \right)^n - \left(57T_e + 24T_i - \frac{9L_t}{k} q_e'' + \frac{6L_t}{k} q_i'' \right)^{n-1} \right] = \frac{\Delta t}{2} \left[\left(-T_e + T_i + \frac{L_t}{k} q_e'' \right)^n + \left(-T_e + T_i + \frac{L_t}{k} q_e'' \right)^{n-1} \right], \quad (1)$$

$$\frac{1}{162k} L_t^2 \rho C_p \left[\left(24T_e + 57T_i - \frac{6L_t}{k} q_e'' + \frac{9L_t}{k} q_i'' \right)^n - \left(24T_e + 57T_i - \frac{6L_t}{k} q_e'' + \frac{9L_t}{k} q_i'' \right)^{n-1} \right] = \frac{\Delta t}{2} \left[\left(T_e - T_i - \frac{L_t}{k} q_i'' \right)^n + \left(T_e - T_i - \frac{L_t}{k} q_i'' \right)^{n-1} \right], \quad (2)$$

in which k is the thermal conductivity of the construction layer, ρ , C_p are the density and specific heat capacity of the wall layer, L_t is the thickness, T_e and T_i are the outside and inside surface temperatures, q_e'' and q_i'' are the outside and inside surface heat fluxes (see Fig. 2), Δt is the time interval between measurements, n and $n - 1$ represent the current and past time instants.

According to Eqs. (1) and (2), if the temperature and heat flux at both the outer and inner construction material layer surfaces are known, the thermal capacitance (ρC_p) and thermal conductivity can be solved as follows:

$$\frac{L_t}{k} = \frac{-b \pm \sqrt{b^2 - 4ac}}{2a} \quad (3)$$

In which $a = a_2 d_2 - c_2 b_2$, $b = a_1 d_2 + a_2 d_1 - (b_1 c_2 + b_2 c_1)$, $c = a_1 d_1 - b_1 c_1$ and $a_1 = (57T_e + 24T_i)^n - (57T_e + 24T_i)^{n-1}$, $a_2 = (-9q_e'' + 6q_i'')^n - (-9q_e'' + 6q_i'')^{n-1}$, $b_1 = (-T_e + T_i)^n + (-T_e + T_i)^{n-1}$, $b_2 = (q_e'')^n + (q_e'')^{n-1}$, $c_1 = (24T_e + 57T_i)^n - (24T_e + 57T_i)^{n-1}$,

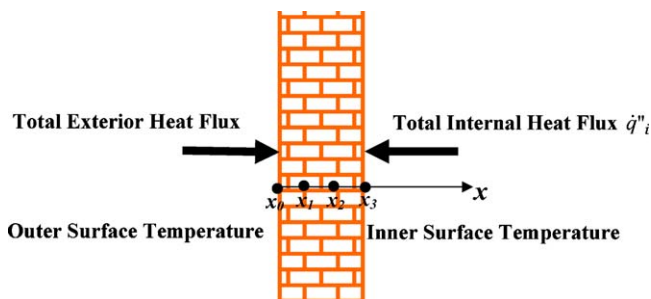


Fig. 2. Configuration of a single brick wall.

$$c_2 = (-6q_e'' + 9q_i'')^n - (-6q_e'' + 9q_i'')^{n-1}, \quad d_1 = (T_e - T_i)^n + (T_e - T_i)^{n-1}, \text{ and } d_2 = -(q_i'')^n - (q_i'')^{n-1}.$$

Substituting Eq. (3) into Eq. (1), the thermal capacitance can be obtained.

3.2. Using the complex Fourier analysis to determine the thermal capacitance and thermal conductivity

According to Luo et al. [17], the temperature at any location through a building wall can be expressed through the following complex Fourier analysis:

$$T(x, t) = A + Bx + \sum_{i=1}^N (A_i e^{\sqrt{j\omega_i/\alpha}x} + B_i e^{-\sqrt{j\omega_i/\alpha}x}) e^{j\omega_i t} = A + Bx + \sum_{i=1}^N C_{Ti}(x) e^{j\omega_i t} \quad (4)$$

In which A , B are the complex Fourier expansion coefficients, j is the imaginary unit and C_{Ti} is the complex temperature amplitude for the angular frequency ω_i . When $x \rightarrow \infty$, $T(x, t)$ should be limited, leading to that $A_i = 0$, $B = 0$.

$$Q(x, t) = \sum_{i=1}^N k B_i \sqrt{\frac{j\omega_i}{\alpha}} e^{-\sqrt{j\omega_i/\alpha}x} e^{j\omega_i t} = \sum_{i=1}^N B_i \sqrt{j\omega_i k \rho C_p} e^{-\sqrt{j\omega_i/\alpha}x} e^{j\omega_i t} = \sum_{i=1}^N C_{Qi}(x) e^{j\omega_i t} \quad (5)$$

where C_{Qi} is the complex heat flux amplitude for angular frequency ω_i . Assuming $H = \sqrt{j\omega_i/\alpha}L_t$, $R = L_t/k$, then the following expression can be obtained:

$$\begin{pmatrix} T_L \\ Q_L \end{pmatrix} = \begin{pmatrix} \cosh(H) & -R \sinh(H)/H \\ -H \sinh(H)/R & \cosh(H) \end{pmatrix} \begin{pmatrix} T_0 \\ Q_0 \end{pmatrix} = \begin{pmatrix} a_{11} & a_{12} \\ a_{21} & a_{22} \end{pmatrix} \begin{pmatrix} T_0 \\ Q_0 \end{pmatrix} \quad (6)$$

In which T_0 , Q_0 and T_L , Q_L are the complex amplitudes of temperature and heat flux on the outer and inner surfaces as defined in Eqs. (4) and (5).

Rearranging Eq. (6), Q_0 and Q_L can be expressed as:

$$Q_0 = -\frac{a_{11}}{a_{12}} T_0 + \frac{1}{a_{12}} T_L = \frac{H}{R \sinh(H)} (\cosh(H) T_0 - T_L) \quad (7)$$

$$Q_L = -\frac{1}{a_{12}} T_0 + \frac{a_{22}}{a_{12}} T_L = \frac{H}{R \sinh(H)} (T_0 - \cosh(H) T_L) \quad (8)$$

Combining Eqs. (7) and (8), $\cosh(H)$ and thermal resistance equate to:

$$\cosh(H) = \frac{Q_0 T_0 + Q_L T_L}{Q_0 T_L + Q_0 T_0} \quad (9)$$

$$R = -\frac{a_{11}}{a_{12}}T_0 + \frac{1}{a_{12}}T_L = \frac{H}{Q_0 \sinh(H)}(\cosh(H)T_0 - T_L) \quad (10)$$

Accordingly, the thermal capacitance and thermal conductivity can be obtained as follows:

$$k = \frac{L_t}{R} \quad (11)$$

$$\rho C_p = \frac{|H|^2 k}{\omega_i^2 L_t^2} \quad (12)$$

3.3. Calculating convective heat transfer coefficient on a room inner surface by the fitting method

From the experimental measurements, the total heat flux and temperature at the centre of all internal room surfaces have been recorded since March, 2003. The total heat flux on any room surface can be expressed as,

$$\dot{q}_{ti}'' = \frac{1}{A_i} \sum_{j=1, j \neq i}^6 \sigma S_{ij}(T_j^4 - T_{ra}^4) + h_i(T_i - T_{ra}) \quad (13)$$

where sub-index i represents the surface in which the total heat flux is calculated, j is the other internal room surfaces, ra is the room air, h_i is the convective heat transfer between the i th wall surface and the room air, S_{ij} is total exchange area between surface i and j calculated according to Hottel and Sarofim [18] and tabulated in Table 2 for a room of size 5.44 m × 5.44 m and height 2.4 m.

Based on Eq. (13), the convective heat flux on a room surface can be obtained by

$$\dot{q}_{conv-i}'' = \dot{q}_{ti}'' - \frac{1}{A_i} \sum_{j=1, j \neq i}^6 \sigma S_{ij}(T_j^4 - T_{ra}^4) = h_i(T_i - T_{ra}) \quad (14)$$

3.4. Calculating the convective heat transfer coefficient of an air gap surface by the fitting method

The air gap can be viewed as a special volume constructed only of opposing walls. In this case, the total surface heat fluxes at both wall surfaces are approximately equal with the following assumptions:

- (1) The specific heat capacity of the air gap is negligible compared to the surrounding walls,
- (2) the contributions from the ground and roof are very small and
- (3) both surfaces adjacent to the air gap are parallel to each other.

According to Luo et al. [17], the equations correlating the heat flux and temperature at the ends of the air-gap are:

$$\dot{q}_{s0}'' = \dot{q}_{s1}'' \quad (15)$$

$$\dot{q}_{s0}'' = \frac{h_{s0}h_{s1}}{h_{s0} + h_{s1}}(T_{s0} - T_{s1}) + \frac{\varepsilon_{s0}\varepsilon_{s1}\sigma(T_{s0}^4 - T_{s1}^4)}{\varepsilon_{s0} + \varepsilon_{s1} - \varepsilon_{s0}\varepsilon_{s1}} \quad (16)$$

In which h is the convective heat transfer coefficient, the thermal radiation absorptivity, subscript $s0$ is the left wall surface (representing the outer surface) and $s1$ corresponds to the right wall surface (the inner surface). Eqs. (15) and (16) are valid at any time. From Eq. (16), the overall heat transfer coefficient for the air gap reads

$$U_{airgap} = \frac{h_{s0}h_{s1}}{h_{s0} + h_{s1}} + \frac{\varepsilon_{s0}\varepsilon_{s1}\sigma(T_{s0}^2 + T_{s1}^2)(T_{s0} + T_{s1})}{\varepsilon_{s0} + \varepsilon_{s1} - \varepsilon_{s0}\varepsilon_{s1}} \quad (17)$$

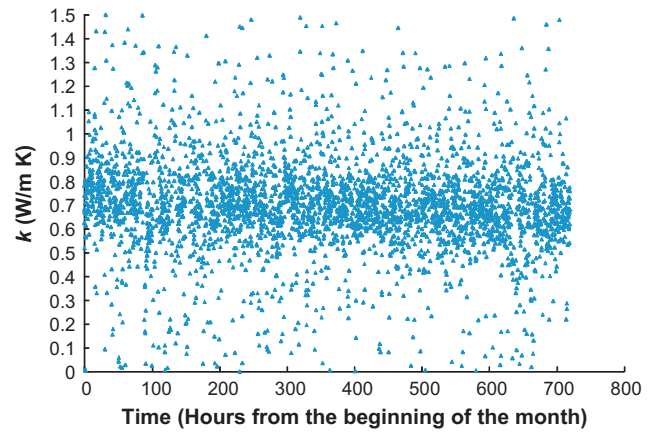


Fig. 3. Calculated instant thermal conductivity for a 110 mm brick layer using the finite volume method in December, 2003 on the campus of the University of Newcastle.

4. Results and discussion

4.1. Thermal capacitance and thermal conductivity from the finite volume scheme and complex Fourier analysis

For the finite volume method (FVM), the thermal capacitance and thermal conductivity are calculated by a Microsoft Excel spreadsheet using Eqs. (1) and (3). The input variables are the monitored temperatures and heat fluxes on the outer and inner surfaces of a homogeneous construction layer (110 mm brick layer in this study). The resulting output variables are the thermal capacitance and the thermal conductivity. The time interval is 10 min and thickness of the brick layer is 110 mm. Shown in Fig. 3 is the calculated thermal conductivity for data obtained in December 2003 from the north wall outer skin of the cavity brick module located on the campus of the University of Newcastle, Australia. It can be observed that the thermal conductivity predominately ranges within 0.5–0.9, with an average value of 0.67.

As for the complex Fourier analysis method, the thermal properties are assumed to be constant during the monitored period. The first step is to find the complex Fourier expansion amplitudes for a given temporal-varying surface temperature or heat flux as follows:

$$\phi(t) = X_0 + \sum_{i=1}^N [X_i \cos(\omega_i t) + Y_i \sin(\omega_i t)] \quad (18)$$

$$psd(\omega_i) = \frac{X_i^2 + Y_i^2}{2\pi} \quad (19)$$

In which $\phi(t)$ is a monitored variable (representing either temperature or heat flux), $\omega_i = i(2\pi/P)$, P is the monitored period (for the December, 2003, $P = 744$ h), i is an integer and psd is the power spectral density. Accordingly, the complex amplitude is constructed as $X_i - jY_i$, in which j is the complex imaginary unit. A program was developed to use Eqs. (9)–(12) to calculate the thermal capacitance and thermal conductivity using input variables from the monitored temperatures and heat fluxes at both the outer and inner surfaces.

Fig. 4 shows the distribution of power spectral density for the outer surface temperature in terms of angular frequency ($\omega_i = 2\pi/P_i$, P_i is the period). It can be observed that the psd peak occurs at a period of 24 h. Therefore, the complex amplitudes corresponding to the period are used to calculate the thermal properties using Eqs. (9) and (10). The final calculated results are listed in Table 1 and shows that the thermal conductivity and thermal capacitance for the 110 mm brick layer for both northern and eastern walls are similar. The average thermal conductivity and thermal capaci-

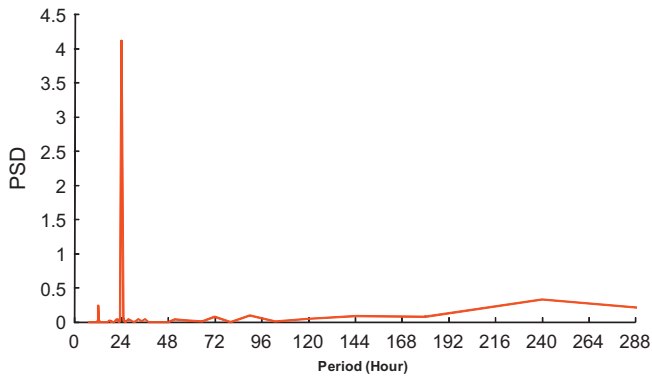


Fig. 4. Power spectral density (PSD) for the temperature on the outer north wall surface of the cavity brick module in December, 2003.

tance calculated by the FVM method are also listed in Table 1 and indicate that the difference between the thermal properties for the northern and eastern wall is larger than those using the complex Fourier analysis method. However, all calculated results are within the range specified from ASHRAE [19].

It can be concluded from Table 1 that complex Fourier analysis is the preferred method to be employed for calculating the thermal capacitance and thermal conductivity based on the monitored temperatures and heat fluxes for both the outer and inner surfaces of a construction material layer.

4.2. Room surface CHTC from the linear fitting

Shown in Fig. 5 is the convective heat transfer calculated from Eq. (14) plotted on the y-axis against the temperature difference between the wall surface and the indoor air $T_{ra} - T_w$. The gradient is the convective heat transfer coefficient. Experimentally obtained measurements correspond to the total heat flux value consisting of both radiant and convective components, therefore Eq. (14) is employed for separation. Fig. 7 shows the fitting result between the total heat flux and $T_{ra} - T_w$ for the ground slab surface. Removing the radiant heat flux from the total heat flux, as seen in Fig. 6, improves the fitting between the convective heat flux and the temperature difference $T_{ra} - T_w$. The resulting convective heat transfer coefficients are tabulated in Table 3 for all internal surfaces. The accuracy of the convective heat transfer coefficients depends on the accuracy of the total heat flux sensors. According to the manufacturer of the Captec sensors, accuracy of the total heat flux sensor on calibration is approximately $\pm 5\%$.

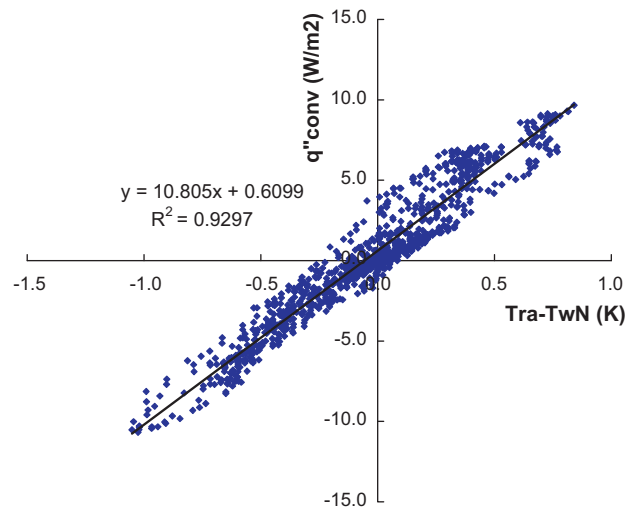


Fig. 5. Linear correlation between $q''_{conv,N}$ and $T_{ra} - T_{w,N}$ for north wall of the cavity brick module from 14 to 21 November, 2003.

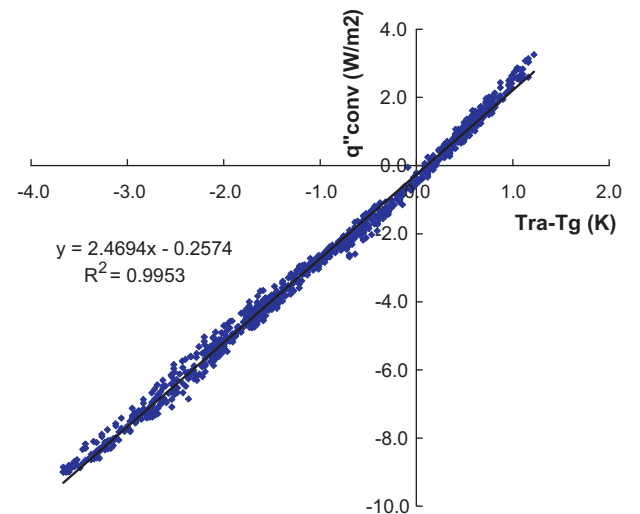


Fig. 6. Linear correlation between $q''_{conv,G}$ and $T_{ra} - T_{w,G}$ for the ground floor of the cavity brick module from 14 to 21 November, 2003.

Table 1

Comparison of thermal capacitance and thermal conductivity obtained by finite volume and complex Fourier analysis methods.

Methods	ρC_p north exterior skin (kJ/m ³ K)	ρC_p east exterior skin (kJ/m ³ K)	k north exterior skin (W/m K)	k east exterior skin (W/m K)
Average from finite volume method	1419	1505	0.67	0.62
Complex Fourier analysis	1242	1257	0.71	0.73
ASHRAE [19]	884.8–1896	884.8–1896	0.36–1.470	0.36–1.470

Table 2

Total exchange area S_{ij} (m²).

	North wall	East wall	South wall	West wall	Roof	Ground
North wall	0.0000	1.4856	1.3406	1.4856	1.4678	1.4678
East wall	1.4856	0.0000	1.4856	1.3406	1.4678	1.4678
South wall	1.3406	1.4856	0.0000	1.4856	1.4678	1.4678
West wall	1.4856	1.3406	1.4856	0.0000	1.4678	1.4678
Roof	1.4675	1.4675	1.4675	1.4675	0.0000	1.6908
Ground	1.4675	1.4675	1.4675	1.4675	1.6908	0.0000

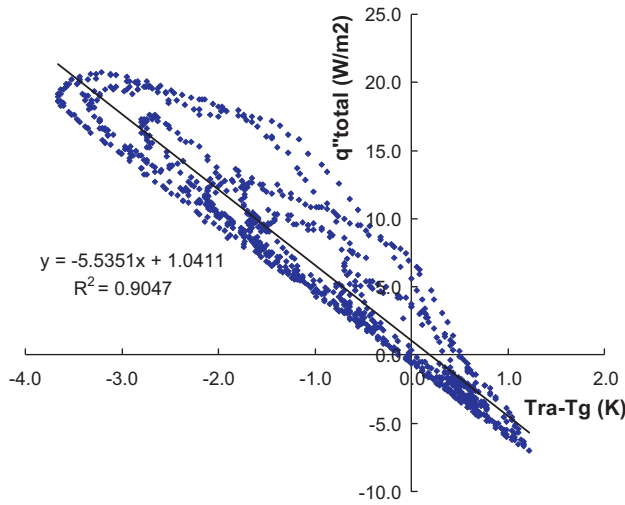


Fig. 7. Linear correlation between $\dot{q}''_{total,G}$ and $T_{ra} - T_{w,G}$ for the ground floor of the cavity brick module from 14 to 21 November, 2003.

4.3. Air gap surface CHTC from the linear fitting

The air gap surface CHTC is obtained through the following two steps:

- (1) Linear fitting of the total surface heat flux as a function of the temperature difference between outer and inner air gap wall surfaces to derive the overall heat transfer coefficient U .
- (2) Deriving the ratio of the CHTC h_{s1}/h_{s0} by determining the correlation between $(T_{s0} - T_{airgap})$ and $(T_{airgap} - T_{s1})$ based on the equation $q_{conv} = h_{s0}(T_{s0} - T_{airgap}) = h_{s1}(T_{airgap} - T_{s1})$.

From step 1, the overall convective heat transfer coefficient U_{conv} for the air gap can be obtained by $U_{conv} = U_{airgap} - U_{thermalR}$, where U_{airgap} is the overall heat transfer coefficient for the air gap and $U_{thermalR}$ is the thermal radiation heat transfer coefficient. The thermal radiation heat transfer coefficient is approximated by assuming a temperature of 20 °C or 293.15 K for both the inner and outer surfaces. Fig. 8 shows the variation of the surface heat flux with respect to $T_{s0} - T_{s1}$, along with the slope of the fitted line representing the overall heat transfer coefficient. It can be observed that the linear fitting of R^2 is over 99%, indicating that the variation of the overall heat transfer coefficient U_{airgap} due to the varying surface temperature, can be ignored. The Kelvin unit for surface temperatures in Eq. (11) eased the effect of varying surface temperatures on U_{airgap} . Table 4 presents the overall heat transfer coefficients for the northern, eastern and western wall air gaps for typical seasonal months. U_{airgap} remains relatively steady for the northern air gap. For the eastern air gap U_{airgap} oscillates between 5.3 and 8.221 W/m² K, and between 6.071 and 7.15 W/m² K for the western wall air gap.

Shown in Fig. 9 is the variation of the $T_{s0} - T_{airgap}$ with respect to $T_{airgap} - T_{s1}$, indicating that the fitting is not as good as in Fig. 8. There are several factors behind the relatively poor linear fitting: (1) the convective heat transfer coefficient is not constant over the one month period; (2) vertical heat flow affects the 1D assumption;

Table 3

The convective heat transfer coefficients for the 6 surfaces of the brick cavity module using weekly measurements (other data available at request).

Time period	North wall	East wall	South wall	West wall	Ceiling	Ground
14/11/2003–21/11/2003	10.805	11.965	11.698	11.188	1.3558	2.4694
28/3/2003–04/04/2003	10.83	10.386	9.0445	10.474	1.3748 ^a	2.6953

^a Indicate that the fitting R^2 is less than 0.9.

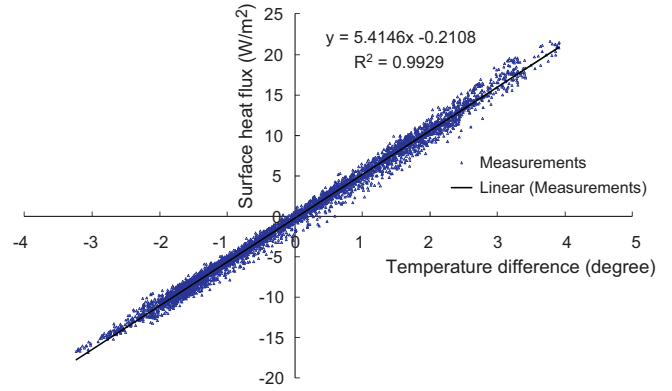


Fig. 8. Linear correlation between $\dot{q}''_{w,G}$ and $T_{outer} - T_{inner}$ for the north wall air gap of the cavity brick module in November, 2003.

Table 4

Fitted overall heat transfer coefficients for air gaps in the cavity brick module for typical seasonal months (other data available at request).

Month	Year	$U_{airgap,north}$	$U_{airgap,east}$	$U_{airgap,west}$
3	2003	5.881	5.883	6.616
6	2004	5.987	6.980	6.233
9	2003	5.870	5.830	6.263
12	2003	5.764	7.981	7.150
Annual average		5.783	6.765	6.581

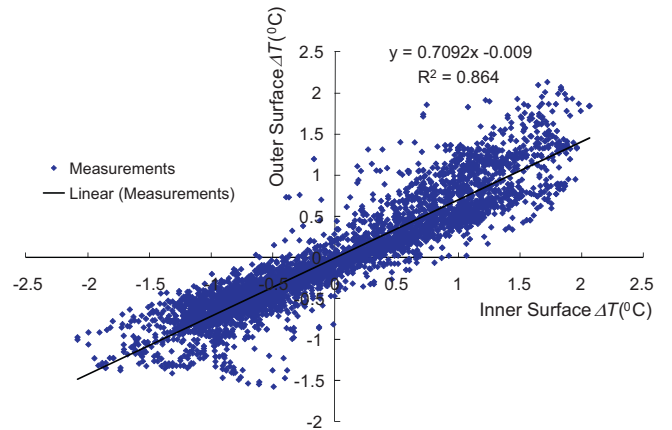


Fig. 9. Linear correlation between $T_{s0} - T_{airgap}$ and $T_{airgap} - T_{s1}$ for the north wall air gap of the cavity brick module in November, 2003.

tion; (3) heat gain or loss at the ground or the ceiling. Based on the $h_{s1}/h_{s0} = 0.7092$ from Fig. 9 and $U_{airgap} = 5.4146$ W/m² K from Fig. 8, h_{s1} and h_{s0} can be calculated according to Eq. (11) with the thermal radiation absorptivity $\epsilon_{s0} = \epsilon_{s1} = 0.9$ and the fixed surface temperature $T_{s0} = T_{s1} = 20$ °C = 293.15 K.

4.4. Surface heat flux predictions using thermal properties from ASHRAE and the fitted results

To examine the effect of the accuracy of the thermal properties of building materials on the numerical predictions for the surface

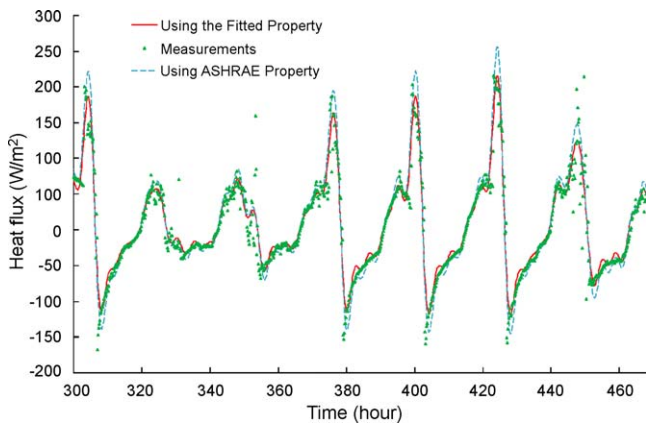


Fig. 10. Comparison of the predicted outer surface heat flux of the outer skin of the cavity brick wall using thermal properties from the present study and ASHRAE handbook with the measurements in December, 2003 on the campus of the University of Newcastle, Australia.

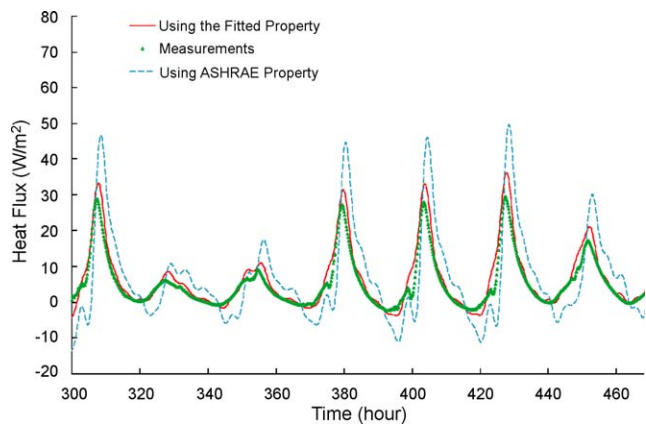


Fig. 11. Comparison of the predicted inner surface heat flux of the outer skin of the cavity brick wall using thermal properties from the present study and ASHRAE handbook with the measurements in December, 2003 on the campus of the University of Newcastle, Australia.

heat fluxes on the building walls, the fitted and ASHRAE thermal capacitance and thermal conductivity for the brick layer were used to calculate the surface heat fluxes for the single-layer brick wall with the monitored outer/inner surface temperatures as the input. For details, refer to Luo et al. [17]. The final predictions using the present and ASHRAE thermal properties are compared with the measurements as shown in Figs. 10 and 11. Figs. 10 and 11 are the comparison of outer and inner surface heat fluxes respectively using both the ASHRAE thermal properties for general brick and the present numerically fitted properties. This comparison indicates that the results using the fitted properties agree better with the measurements than the ASHRAE table.

5. Conclusions

Using the annually monitored thermal performance data sourced from the experimental measurements taken at the campus of the University of Newcastle, Australia, the in-situ time varying thermal capacitance and thermal conductivity are determined by the finite volume method, with the constant thermal properties

calculated by the complex Fourier analysis method. The difference in thermal properties for the northern and eastern outer brick layers is smaller for the complex Fourier analysis method than for the finite volume method. The overall heat transfer coefficient of the air gap and convective heat transfer coefficients for room wall surfaces have been obtained using a linear fitting method. All calculated results are within the range of published data. Using the convective heat transfer flux obtained by removing the thermal radiation flux from the total heat flux, improves numerical fitting greatly. The numerical predictions using the calculated thermal properties agree better with the measurements than the properties from the ASHRAE handbook.

Acknowledgements

This work has been supported by Think Brick Australia (formally the Clay Brick and Paver Institute) and the Australian Research Council. The support of both organisations is gratefully acknowledged.

References

- [1] ASTM C518-04, Standard Test Method for Steady-State Thermal Transmission Properties by Means of the Heat Flow Meter Apparatus, 2004.
- [2] ASTM C1363-05, Standard Test Method for Thermal Performance of Building Materials and Envelope Assemblies by Means of a Hot Box Apparatus, 2005.
- [3] S.E. Gustafsson, Transient plane source techniques for thermal conductivity and thermal diffusivity measurements of solid materials, *Review of Scientific Instruments* 62 (3) (1991) 797.
- [4] A. Bouguerra, A. Ait-Mokhtar, O. Amiri, M.B. Diop, Measurement of thermal conductivity, thermal diffusivity and heat capacity of highly porous building materials using transient plane source technique, *International Communications in Heat and Mass Transfer* 28 (8) (2001) 1065–1078.
- [5] K.W. Ghazi, B. Binder, R. Vonbank, A simple method to determine the specific heat capacity of thermal insulations used in building construction, *Energy and Buildings* 35 (2003) 413–415.
- [6] O. Carpentier, D. Defer, E. Antczak, A. Chauchois, B. Duthoit, In situ thermal properties characterization using frequential methods, *Energy and Buildings* 40 (3) (2008) 300–307.
- [7] C. Peng, Z. Wu, In situ measuring and evaluating the thermal resistance of building construction, *Energy and Buildings* 40 (11) (2008) 2076–2082.
- [8] M. Cucumo, A.D. Rosa, V. Ferraro, D. Kaliakatsos, V. Marinelli, A method for the experimental evaluation in situ of the wall conductance, *Energy and Buildings* 38 (3) (2006) 238–244.
- [9] M.G. Emmel, M.O. Abadie, N. Mendes, New external convective heat transfer coefficient correlations for isolated low-rise buildings, *Energy and Buildings* 39 (3) (2007) 335–342.
- [10] A. Hagishima, J. Tanimoto, Field measurements for estimating the convective heat transfer coefficient at building surfaces, *Building and Environment* 38 (7) (2003) 873–881.
- [11] S.E.G. Jayamaha, N.E. Wijeyesundera, S.K. Chou, Measurement of the heat transfer coefficient for walls, *Building and Environment* 31 (5) (1996) 399–407.
- [12] Y. Liu, D.J. Harris, Full-scale measurements of convective coefficient on external surface of a low-rise building in sheltered conditions, *Building and Environment* 42 (7) (2007) 2718–2736.
- [13] J. Shao, J. Liu, J. Zhao, W. Zhang, D. Sun, Z. Fu, A novel method for full-scale measurement of the external convective heat transfer coefficient for building horizontal roof, *Energy and Buildings* 41 (8) (2009) 840–847.
- [14] A.D. Irving, T. Dewson, G. Hong, B. Day, Time series estimation of convective heat transfer coefficients, *Building and Environment* 29 (1) (1994) 89–96.
- [15] S.R. Delaforce, E.R. Hitchin, D.M.T. Watson, Convective heat transfer at internal surfaces, *Building and Environment* 28 (2) (1993) 211–220.
- [16] C. Luo, B. Moghtaderi, B. Sugo, A. Page, A new stable finite volume method for predicting thermal performance of a whole building, *Building and Environment* 43 (2008) 37–43.
- [17] C. Luo, B. Moghtaderi, A. Page, Modelling of wall heat transfer using modified conduction transfer function, finite volume and complex Fourier analysis methods, *Energy and Buildings* 42 (5) (2010) 605–617.
- [18] H.C. Hottel, A.F. Sarofim, *Radiative transfer McGraw-Hill series in mechanical engineering*, McGraw-Hill, New York, 1967.
- [19] ASHRAE, *Handbook of Fundamentals*, American Society of Heating, Refrigeration and Air Conditioning Engineers, Atlanta, GA, 2001.